Molecular Orientation in Dry and Hydrated Cellulose Fibers: A Coherent Anti-Stokes Raman Scattering Microscopy Study

Maxwell Zimmerley,[†] Rebecca Younger,[†] Tiffany Valenton,[†] David C. Oertel,[‡] Jimmie L. Ward,[§] and Eric O. Potma*[,†]

Department of Chemistry, University of California, Irvine, California 92697, The Procter & Gamble Company, 8700 Mason-Montgomery Road, Mason, Ohio 45040, and The Procter & Gamble Company, 11510 Reed Hartman Highway, Cincinnati, Ohio 45241

Received: April 9, 2010; Revised Manuscript Received: May 25, 2010

Coherent anti-Stokes Raman scattering (CARS) microscopy is combined with spontaneous Raman scattering microspectroscopy and second harmonic generation (SHG) microscopy to interrogate the molecular alignment in dry and hydrated cellulose fibers. Two types of cellulose were investigated: natural cellulose I in cotton fibers and regenerated cellulose II in rayon fibers. On the basis of the orientation of the methylene symmetric stretching vibration, the molecular alignment of cellulose microfibrils is found to be conserved on the micrometer scale. Whereas the molecular orientation in cotton shows modest variability along the fiber, the alignment of the cellulose units in rayon is highly consistent throughout the fiber. The ordered alignment is retained upon fiber hydration. Upon hydration of the cellulose fibers, an anisotropic electronic contribution is observed, which indicates an ordered incorporation of water molecules into the fiber structure. The third-order and second-order electronic polarizability of cellulose I are directed along the axis of the polyglucan chain. No second-order optical response is observed in cellulose II, supporting the antiparallel arrangement of the polyglucan chains in regenerated cellulose.

1. Introduction

Cyrstalline cellulose occurs naturally as one of two structures: triclinic cellulose I_α and monoclinic cellulose I_β.[1] The other common cellulose crystal structure, designated cellulose II, is formed either through mercerization or regeneration and like cellulose I_β has a monoclinic crystal structure. Whereas these different forms of cellulose are chemically identical, the different packing and orientation of the crystallites (microfibrils) on the microscopic scale translates into marked differences in the mesoscopic and macroscopic properties of the fibers such as the crystal modulus[2] and tensile strength.[3]

On a microscopic level, cellulose I_α, I_β, and II exhibit domains of highly ordered crystalline cellulose alongside regions of less-ordered amorphous cellulose. The ordered microcrystalline domains generally have widths on the order of nanometers and lengths on the order of tens of nanometers.[1] The degree of crystallinity and the orientation of the crystalline and amorphous domains of both synthetic and natural cellulose fibers are known to affect macroscopic mechanical properties.[4−6] Indeed, one of the benefits of producing regenerated fibers is the ability to exert greater control over the bulk properties affected by orientation.[4]

Cellulose is hydrophilic and the presence of water is known to affect the bulk properties of natural and synthetic fibers and films through changes in both the crystalline and amorphous domains. Dehydration of natural fibers has been shown to decrease the crystallinity[5] and the order[6] of the crystalline domains in never-dried cotton. This loss can be controlled to some extent by slowly drying cotton at high temperatures, as demonstrated by Iyer et al., who were able to retain a higher degree of crystallinity of the fibers in the final dry state. More recently, nuclear magnetic resonance measurements have shown that rehydration induces an increase of crystallization and order in both the crystalline and amorphous regions of cellulose fibers.[7] Whereas it is known that water increases orientation and crystallinity of the fibers in general, it is less well understood whether rehydration induces changes that are continuous throughout the fiber, or whether there are heterogeneously distributed domains with varying degrees of orientation and order.

Common techniques for measuring the orientation of domains include tensile measurements,[3] X-ray diffraction (XRD) techniques,[8,9] and polarized vibrational spectroscopies.[10−13] Recently, Gindl et al. used synchrotron X-ray microbeam diffraction (using a $5 \times 5\ \mu m^2$ beam) to investigate the degree of orientation in cellulose II fibers while unstrained, strained, or bent.[14] They were able to see that, on a bend, the chains are more aligned along the outer edge of the bend than on the inside of the bend. They also obtained a constant value for the degree of orientation across the fiber while unstrained. Kong et al. performed similar measurements using a smaller probing spot (beam waist ~0.5 mm) and were able to observe differences in orientation between the core and the surface of the unstrained regenerated cellulose fibers,[15] in accordance with previous experiments by Eichorn et al.[16] The increase in understanding gained by using the smaller probing volumes highlights the need for higher resolution in investigating the crystalline properties of cellulose fibers.

While XRD techniques provide direct insight into the orientation of cellulose chains, diffraction patterns are typically attained only from selected spots in the cellulose specimen. More insight in the distribution of domain size and molecular orientation throughout the fiber requires microscopic imaging

* To whom correspondence should be addressed. Tel: 949-824-9942. Fax: 949-824-8571. E-mail: epotma@uci.edu.
[†] University of California, Irvine.
[‡] The Procter & Gamble Company, Mason, Ohio.
[§] The Procter & Gamble Company, Cincinnati, Ohio.

10.1021/jp103216j
Published on Web 07/12/2010

with sufficient sensitivity to molecular alignment. Optical methods based on vibrational spectroscopy are ideal candidates for this purpose. The directional dependence of vibrational signals generated in cellulose by polarized light has been well established with both IR[17] and Raman[18] spectroscopy. Polarized vibrational spectroscopy measurements have been correlated with the orientation of specific chemical bonds relative to the orientation of the cellulose fiber.[13,19] In Raman spectroscopy, strong anisotropies exist in the C−H stretching and C−O−C regions near 2900 and 1095 cm^{-1} respectively, which have been used to investigate the average orientation of the chemical bonds throughout the fiber. The maximum Raman polarizability of the CH stretching mode was found in the direction perpendicular to the fiber axis, whereas the polarizability of the COC mode is directed along the long axis of the fiber.[20,21] An attractive advantage of the Raman spectroscopic approach is that such orientation parameters can be obtained from submicrometer probing volumes, with the potential of generating high resolution maps based on contrast derived from molecular orientation. Such molecular alignment maps are highly desirable as they not only offer a direct view of the structural differences on the submicrometer scale between the distinct forms of cellulose but also provide insight into how these structural parameters change as a function of external agents. The latter capability can be relevant to advancing the understanding of the mechanisms that underlie the process of structural degradation of cellulose for the purpose of ethanol biofuel production.

In this work, we perform a Raman-based study of molecular orientation in cellulose fibers by making use of coherent anti-Stokes Raman scattering (CARS) microscopy.[22−24] The CARS technique enables vibrational imaging at much higher image acquisition rates compared to spontaneous Raman scattering, and is thus a preferred vibrational imaging method for generating maps at submicrometer resolution and with high pixel density. A Raman-sensitive technique, CARS provides similar sensitivity to molecular orientation as probed in conventional polarization-sensitive Raman spectroscopy. CARS microscopy has been successfully used to image molecular orientation in lipid bilayer systems[25,26] and to probe vibrational anisotropy in liquid crystals.[27,28] In addition to vibrational sensitivity, the CARS technique is also sensitive to changes in the electronic polarizability. This latter capability is useful for monitoring changes in the electronic anisotropy of molecular systems, which is particularly relevant for the highly aligned cellulose polyglucan molecular chains.

We employ CARS microscopy to map out the orientation of the CH_2− and CH-stretching vibrational region, both in natural (cotton) and in synthetic (rayon) cellulose fibers. On the basis of CARS polarization data acquired from each pixel, we generate images sensitive to anisotropy and orientation of the polyglucan chains in cotton and rayon fibers, either dry or hydrated. In addition, we correlate the CARS data with Raman spectroscopic point measurements to confirm the molecular mode orientation, and with second harmonic generation (SHG)[29,30] images to investigate the electronic polarizability of the cellulose units. On the basis of these combined studies, we draw conclusions on molecular alignment in cotton and rayon fibers before and after hydration.

2. Experimental Section

2.1. Materials

In this study, we use cotton as a representative cellulose I material. Cotton fibers were extracted from cotton swabs (Kendall Q-tips, Tyco Healthcare). Cotton consists of >90% cellulose, specifically in the I_β form, in addition to water and small traces (<1%) of waxes and pectins. We use regenerated rayon fiber as a representative cellulose II material. The rayon fibers used in this study were provided by The Procter and Gamble Company. Dry fibers were sandwiched between two glass coverslips. A small piece of 170 μm thick glass was placed adjacent to the fiber for the purpose of normalizing the CARS signal. To prevent motion of the fibers, the coverslips were sealed with epoxy, which allowed for day-long imaging sessions without significant movement of the fibers. Hydrated fibers were soaked in Millipore water for 2 days and imaged immersed in water. For these images, no glass was placed in the focal plane and the water bulk was used to normalize the CARS signal.

2.2. CARS Microscopy. Pump and Stokes beams for CARS microscopy were generated with a picosecond optical parametric oscillator (OPO) (Levante Emerald, APE, Germany) system pumped by a 1064 nm, picosecond Nd:vanadate laser (PicoTrain, High-Q, Austria). The 750−950 nm pulsed radiation from the OPO served as the pump beam in the CARS excitation process, whereas the residual 1064 nm light was used as the Stokes beam. In this study, the pump and Stokes beams are parallel polarized. Before entering the microscope, the spatially and temporally overlapped pulses passed through an achromatic half-wave plate to control the excitation polarization. Imaging was performed with a galvanometric scan head (Olympus Fluoview 300) interfaced with an inverted microscope (Olympus IX-71). A 20×, 0.75 NA dry objective lens was used in these imaging studies. The CARS focal volume in these studies has a lateral diameter of ∼0.5 μm and an axial depth of ∼3.5 μm. The CARS signal was detected in the forward direction through two bandpass filters (652 nm, 40 nm bandwidth, Chroma) on a red-sensitive photomultiplier tube detector (R3896, Hamamatsu).

Under the polarization conditions chosen, the CARS signal is predominantly linearly polarized, and the signal can be detected without an analyzer. Nonetheless, the polarization state of the excitation beams is slightly distorted when propagating through the microscope optics, resulting in depolarized and elliptically polarized components.[31] The change of the polarization state introduced a modest (∼10%) modulation of the CARS signal when rotating the half-wave plate. To a good approximation, this modulation was corrected by measuring the nonresonant CARS signal of a (isotropic) water solution for every setting of the half-wave plate, and dividing the CARS cellulose signal by the water calibration data. This correction procedure produced the expected isotropic polarization plots for every other liquid tested (dimethyl sulfoxide, cyclohexane) and for the nonresonant glass signal. In addition, this procedure produces CARS polarization plots of cellulose fibers that are consistent with Raman polarization data in the CH stretching range.

The maximum polarization difference of the CARS signal was measured at 2880 cm^{-1}, which is the setting used to generate the polarization plots. CARS spectra were obtained by imaging from 2700 to 3100 cm^{-1} in ∼6−8 cm^{-1} steps at this polarization as well as the polarization orthogonal to it. The signal from the fiber was normalized to either a piece of glass in the same plane for dry fibers or the surrounding water for hydrated fibers.

2.3. SHG Microscopy

Second harmonic generation signals were generated with a 100 fs, 800 nm laser beam derived from a Ti:sapphire laser (Mira 900, Coherent, Mountain View). The 800 nm beam was collinearly aligned with the picosecond CARS excitation beams

through the microscope optics to ensure coregistration of the CARS and the SHG images. SHG signals were detected both in the forward and in the epi- direction through two bandpass filters (400 nm, 40 nm bandwidth, Thorlabs) on a photomultiplier tube (R3896, Hamamastu). We note that no autofluorescence of the cellulose fibers was observed within the spectral detection window. To remove polarization distortion effects, the setup was calibrated by measuring the two-photon excited fluorescence (TPEF) from a concentrated aqueous Rhodamine 6G solution as a function of the half-wave plate setting. The SHG images from the fibers were normalized according to the TPEF calibration profile. Using an analyzer, we verified that there were no spatially dependent polarization variations within the field of view used in these studies (200 × 200 μm for a 20×, 0.75 NA dry lens).

2.4. Raman Microspectroscopy. Raman microspectroscopy was performed with a 532 nm beam derived from a frequency-doubled Nd:vanadate laser (Verdi V5, Coherent, Mountain View). About 10 mW of excitation light was coupled into the microscope through the back-port of the microscope frame (Olympus IX71), and focused by the 20×, 0.75 NA objective lens onto the sample. Switching between CARS/SHG operation and Raman point measurements involved a simple turn of the carousel wheel. Raman-scattered light was detected in the epi-direction and filtered by a holographic notch filter (Kaiser). Raman spectra were recorded with a spectrometer (Shamrock, Andor) interfaced with a cooled CCD camera (iDus DU401A, Andor). Raman spectra were collected with 30s integration times. Raman polarization spectra were obtained by rotating the excitation beam relative to the fiber axis.[32] The polarization of the Raman excitation light was controlled by a 532 nm half-wave plate. Polarization distortions were compensated by calibrating the Raman spectra with the signal acquired from an isotropic liquid (dimethyl sulfoxide) in the 2700 to 3100 cm^{-1} range.

2.5. Image & Data Processing

The procedure for determining chemical bond orientation from CARS images with different incident polarizations was previously developed and utilized to study liquid crystals.[27] Here, we adopt a slightly different approach by fully resolving the CARS signal as a function of the excitation polarization. Polarization plots were obtained by recording 36 CARS images taken at 10° intervals of the excitation polarization orientation. For each pixel (x,y) in the image, the maximum signal as a function of excitation polarization was determined. The maximum signal is denoted by $I_{max}(x,y)$, and the orientation of the excitation polarization associated with this intensity is indicated by $\phi_{max}(x,y)$. Note that $\phi_{max}(x,y)$ may vary from pixel to pixel. The minimum intensity $I_{max}(x,y)$ is determined at $\phi_{max}(x,y) - 90°$. The anisotropy magnitude $\rho(x,y)$ is determined as:

$$\rho(x,y) = \frac{I_{max}(x,y) - I_{min}(x,y)}{I_{max}(x,y) + I_{min}(x,y)} \quad (1)$$

In the procedure outlined above, the chemical bond orientation is expressed in terms of the anisotropy magnitude $\rho(x,y)$ and the director angle $\phi_{max}(x,y)$. This fully polarization-resolved procedure is chosen because the polarization-angle-dependent CARS profile can vary markedly from pixel to pixel. Because of the nonuniformity of the angle-resolved polarization profile, ratiometric imaging based on just two orientations of the incident polarization is insufficient to accurately characterize the chemical bond orientation.

It was found that noise is introduced in the $\rho(x,y)$ images at locations away from the cellulose fiber, where the CARS signals collected are negligible. In the case of negligible CARS signals, in areas where the focal volume resides in air rather than in the fiber, a simple thresholding procedure was applied to remove this background artifact. All image processing was done using macros developed in the *ImageJ* environment, whereas further numerical processing and plotting was performed with *Origin*.

3. Results and Discussion

3.1. Raman and CARS Polarization of Dry Cotton Fibers. Part a of Figure 1 shows a representative spontaneous Raman spectrum in the CH-stretching region obtained from a point measurement in a dry cotton fiber. The spectrum of cotton shows a distinct maximum at 2890 cm^{-1}, a broad spectral feature around 2945 cm^{-1}, and a smaller peak at 2963 cm^{-1}. The Raman spectrum is highly dependent on the orientation of the long axis of the fiber relative to the polarization of the excitation beam. The two spectra displayed in part a of Figure 1 correspond to the Raman spectrum of maximum and minimum intensity as a function of fiber orientation. It is seen that the 2890 cm^{-1} peak is highly orientation dependent, whereas the 2963 cm^{-1} band is relatively insensitive to fiber orientation. Similar observations have been made in cellulose derived from Valonia and Ramie.[32] We assign the 2890 cm^{-1} to the symmetric CH_2 stretch of the methylene groups,[33] which are predominantly aligned orthogonal to the long axis of the polysaccharide chains, resulting in a strong polarization dependence. The preferential orientation is likely mediated by the hydroxyl group, which forms directional hydrogen bonds with adjacent chains. The spectral density in the 2945 to 2963 cm^{-1} range can be largely attributed to the CH stretching vibrations within the pyranose ring, which lack a well-defined projection along the molecular chain axis.

The CARS spectrum in part b of Figure 1 shows the same dependence on fiber orientation as observed in the Raman spectrum. Because of spectral interference with the nonresonant background, the methylene symmetric stretching vibration is shifted somewhat to the red at 2880 cm^{-1}. We will use the strong orientation dependence seen at this vibrational frequency to study the molecular alignment in cellulose fibers using CARS imaging. Note that spectral interferences in the CARS spectrum introduce a significant reduction of the spectral density on the blue side of the 2890 cm^{-1} band, which makes this CARS vibrational range less sensitive to orientation of the CH groups.

In part c of Figure 1, the CARS and Raman signals are plotted as a function of the excitation polarization relative to the long axis of the cotton fiber. To minimize tentative Fresnel effects in the backward scattered Raman signal, the ratio of the methylene stretching vibration (2890 cm^{-1}) over the polarization insensitive band at 2963 cm^{-1} was taken. The resulting Raman ratio signal shows a clear orientation dependence, which shows the preferential orientation of the CH_2 modes relative to the long axis of the fiber. Depending on the location in a given fiber segment, we found that the CH_2 modes are aligned at angles 30° to 90° to the main fiber axis. This heterogeneity indicates that on a microscopic scale the cellulose units are oriented at a variety of angles along the fiber. The CARS polarization dependence reveals a similar pattern.

3.2. Spatial Heterogeneity in Cotton Fibers. Parts a and b of Figure 2 show CARS images of dry cotton fibers taken at 2880 cm^{-1} with different orientations of the incident polarization. A clear orientation dependence is observed. To extract molecular bond orientation information, $\rho(x,y)$ anisotropy and $\phi_{max}(x,y)$ angular maps were generated, as depicted in parts c and d of Figure 2, respectively. The anisotropy image indicates

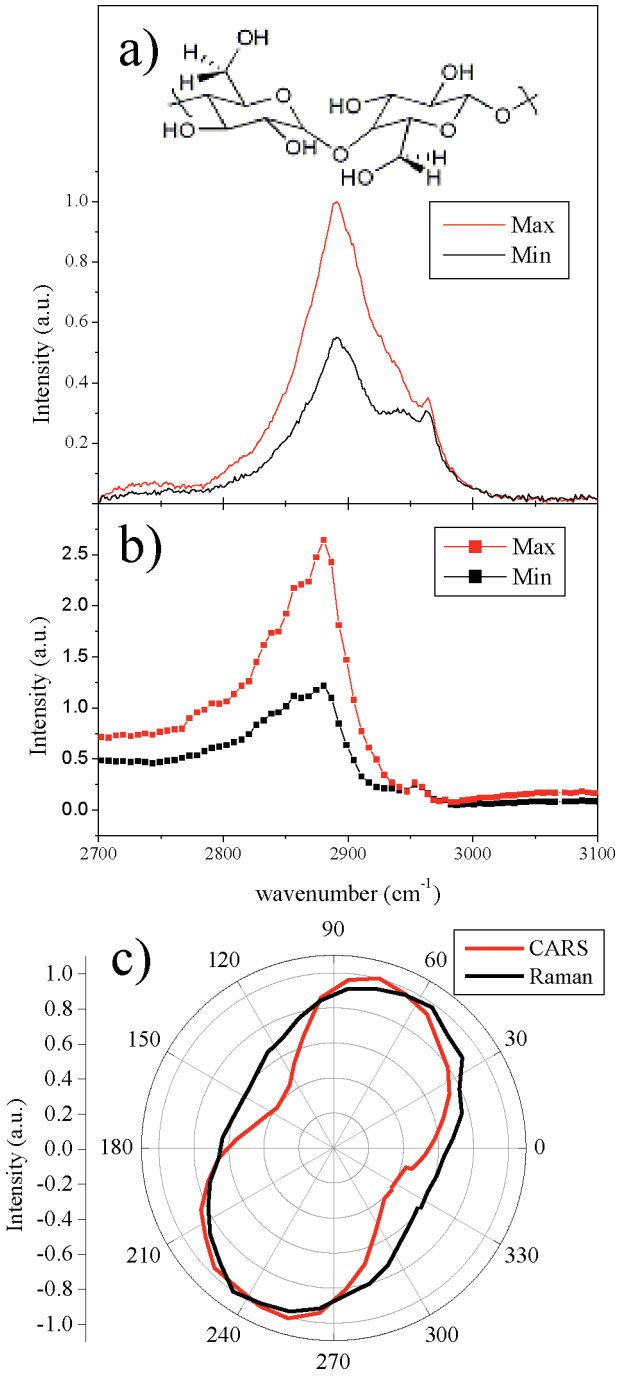

Figure 1. a) Raman spectrum of dry cotton. Red trace corresponds to fiber orientation with maximum Raman response, whereas black trace corresponds to the minimum response 90° rotated from the maximum. Insert shows the structure of cellulose. b) CARS spectrum of dry cotton. Red and black trace correspond to the same orientations as indicated in a). c) Polar plots of the CARS signal at 2880 cm^{-1} (red trace) and the 2890/2963 cm^{-1} ratio of the Raman intensity (black trace).

that the methylene groups have a preferential orientation throughout the fiber. No regions of isotropic orientation of the CH_2 mode were observed anywhere in the fiber. This confirms the relative order of the cellulose units on the microscopic scale. The $\phi_{max}(x,y)$ image shows the preferential orientation of the CH_2 modes in the fiber. The orientation is relatively constant along the fiber, reflecting an ordered arrangement of the linear polyglucan chains throughout.

At several locations in the fiber, however, small regions with different polarization properties were observed. A smaller region is shown magnified in Figure 3, where distinct polarization plots were obtained from several ~5 μm wide areas of the fiber segment. In the region labeled as area 1, the CARS polarization shows a clear orientation of the methylene group. In addition, a small lobe oriented orthogonal to the resonant methylene mode is seen. The two-lobed pattern can be explained by either a strong, anisotropic nonresonant background contribution or by a bimodal distribution of the orientation of the CH_2 mode. As discussed in section 3.5, we attribute the appearance of a second lobe to an anisotropic electronic background. The contribution of this additional electronic component varies from region to region. In area 2 of Figure 3, for instance, the electronic component is particularly strong. Because the electronic polarizability is related to molecular arrangement and packing, the spatial variation of the electronic component indicates that there is a modest spatial heterogeneity of the cellulose structure in the cotton fiber at these length scales.

3.3. SHG of Cotton Fibers. SHG measurements probe the second-order nonlinearity of the electronic polarizability, and thus provide additional insight in the electronic nonlinear response of cellulose. The polarization dependence of the SHG signal from cellulose was measured both in the forward and in the epi-direction. Whereas the SHG signals in both channels exhibit the same trend when rotating the polarization of the excitation beam, the epi-detected signal from the ~20 μm thick dry cotton fibers was observed to be stronger, probably due to a significant backscattered contribution from the forward propagating SHG radiation.[29] In Figure 4, the CARS response from the methylene groups is compared with the SHG response from the fiber. The maximum SHG response from cotton is seen when the excitation polarization is aligned with the long axis of the fiber. Similar observations have been made by Brown et al.[29] Note that the second-order electronic SHG response of the polyglucan chain is directed along the same molecular axis as the third-order electronic response discussed in section 3.2.

3.4. Raman and CARS Polarization of Dry Rayon Fibers. The Raman spectrum of rayon is shown in part a of Figure 5. Similar to cotton a strong contribution of the symmetric CH_2 stretching vibration is seen, in addition to a broader shoulder in the 2950 cm^{-1} range. The distinct peak at 2963 cm^{-1} observed in cotton is less prominent in rayon. The maximum methylene stretching vibration in rayon is attained at 2885 cm^{-1}, at somewhat lower energy than observed in cotton. Both the Raman spectrum and the CARS spectrum, depicted in part b of Figure 5, show a strong fiber orientation dependence. Part c of Figure 5 shows the Raman and CARS polarization plots of the methylene stretching vibration. A clear preferential orientation of the CH_2 mode is seen, aligned 90° with respect to the long axis of the fiber. Unlike in cotton, this alignment is highly conserved throughout the rayon fiber.

Figure 6 shows the CARS anisotropy and $\phi_{max}(x,y)$ images for rayon at 2880 cm^{-1}. The area in the lower half of the image corresponds to the glass coverslip used to calibrate the data. The rayon fiber, displayed in the upper half of the image, shows a relatively constant anisotropy along the fiber (part a of Figure 6). There is some spatial variation in the magnitude of the anisotropy, which could indicate higher and lower degrees of ordering of the methylene bonds. The regions of higher and lower anisotropy magnitude also appear to run parallel to the fiber in distinct bands. These bands may arise due to shear and tensile stress during the drawing process. Despite the anisotropy variation, the $\phi_{max}(x,y)$ image in part b of Figure 6 shows that the orientation of the CH_2 group is largely uniform along the long axis of the fiber, aligned at 90° with respect to the fiber

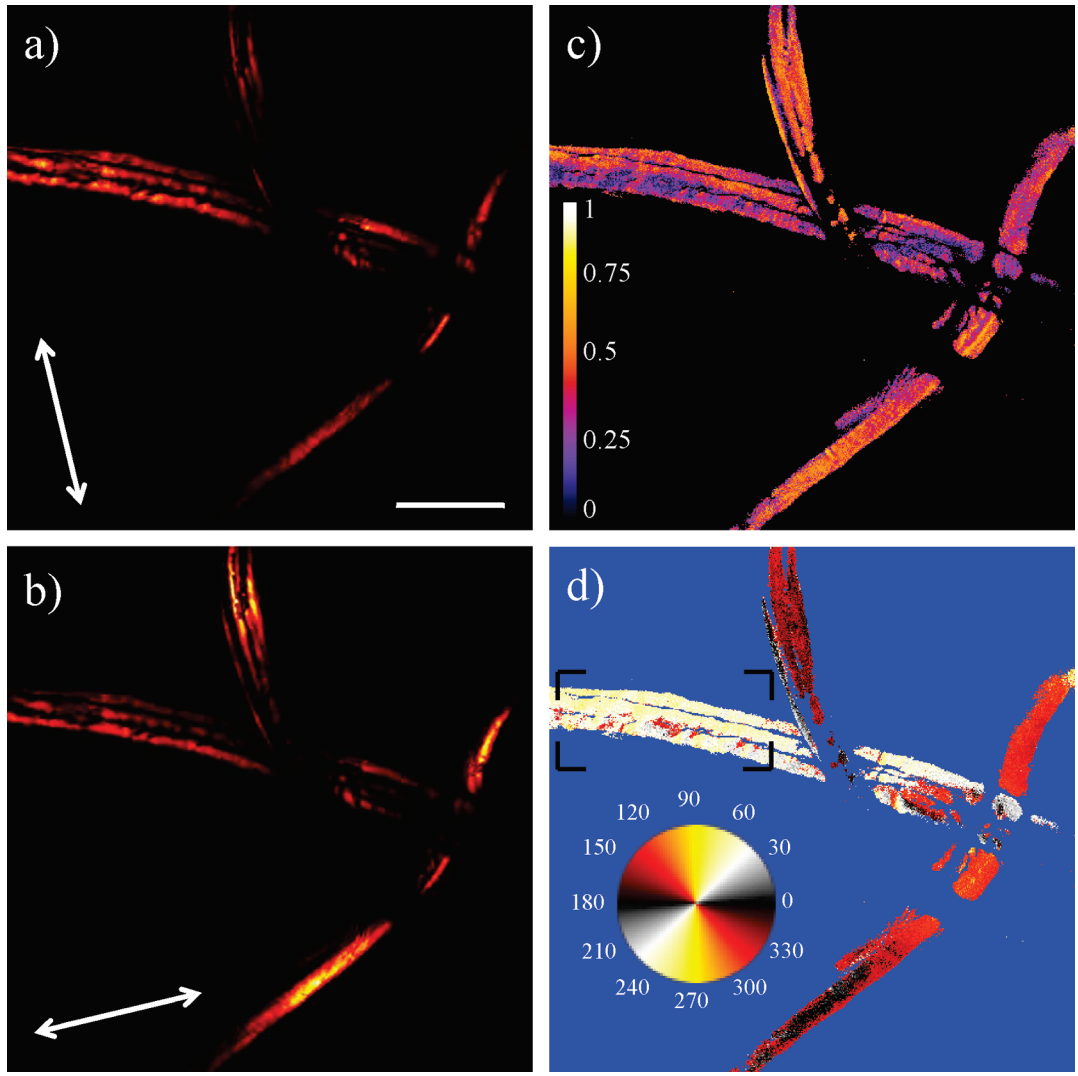

Figure 2. a) CARS image of dry cotton at 2880 cm^{-1}. Incident light polarization orientation is indicated by the arrow. b) Same CARS image taken with incident light orthogonally polarized to the orientation in a). c) The anisotropy magnitude image. d) The director angle image. Images are 512 × 512 pixels and the scale bar is 35 μm.

axis. This is the general trend observed for all dry rayon fibers imaged in this study.

3.5. Comparison of SHG in Cotton and Rayon. In contrast with observations of mercerized cellulose fibers,[30] the regenerated cellulose II fibers used in this study produced no appreciable SHG response under identical imaging conditions with cotton fibers. We note that the CARS signal strengths of the rayon and cotton fibers are of the same magnitude, which indicates that the density of cellulose within the SHG focal volume is comparable for both types of cellulose fibers. This observation suggests that a different molecular arrangement of the polyglucan chains may be responsible for the difference in SHG response. Contrary to cellulose I, in which the polyglucan chains are aligned in a parallel fashion, an antiparallel arrangement has been predicted for cellulose II.[34] We argue below that the difference in alignment of the polymer chains provides a possible explanation for the lack of SHG signal in regenerated cellulose fibers.

Compared to collagen, another biopolymer, the origin of the second-order nonlinearity of cellulose has received relatively little attention. Studies on collagen have indicated that the second-order optical response results from both chiral and achiral contributions.[35] Because cellulose is an array of chiral glucose units, a chiral component to the SHG response may be expected in addition to an achiral component.[36] The achiral contribution is expected to be sensitive to the polar alignment of the polyglucan chains, whereas the chiral contribution should be significantly less sensitive to the difference between parallel and antiparallel chains. The difference between cellulose I (cotton) and regenerated cellulose II (rayon) observed in this study thus confirms that there is a difference in polar alignment of the biopolymer chains between the two forms of cellulose and it suggests that the major component to the second-order response as probed in a conventional SHG imaging experiment is achiral in nature.

3.6. Hydrated Cotton and Rayon. Raman and CARS spectra of wet cotton for the maximum and minimum polarizations are shown in parts a and b of Figure 7, respectively. Upon hydration, the main spectral features in the CH-stretching region are retained. Similarly, the fiber orientation dependence resembles the trends observed for the nonhydrated cotton fibers. The polarization plot in part c of Figure 7 shows that the methylene stretching vibration maintains a preferred orientation with respect to the fiber axis. No clear signs of anisotropy loss were observed. These results indicate that the orientation of the methylene groups is not markedly affected by the interstitial water molecules.

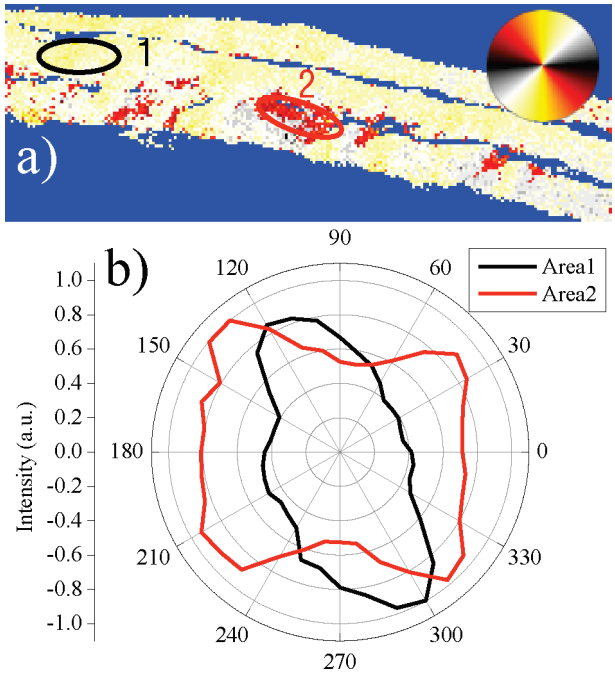

Figure 3. a) Close-up of boxed region from part d of Figure 1. b) CARS polar plots of the two areas indicated in part a.

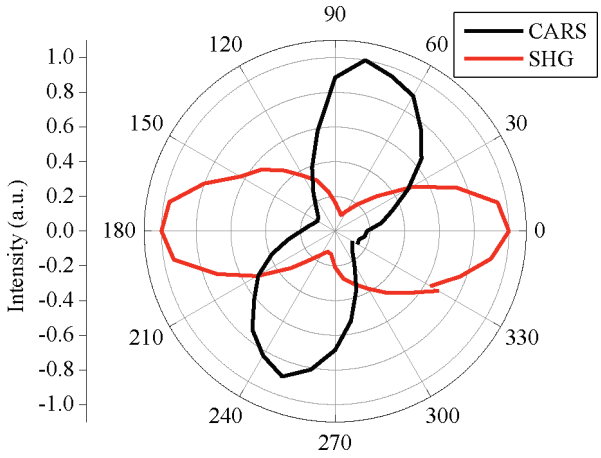

Figure 4. Comparison of the CARS angular dependence at 2880 cm^{-1} and the SHG angular dependence of a single cotton fiber.

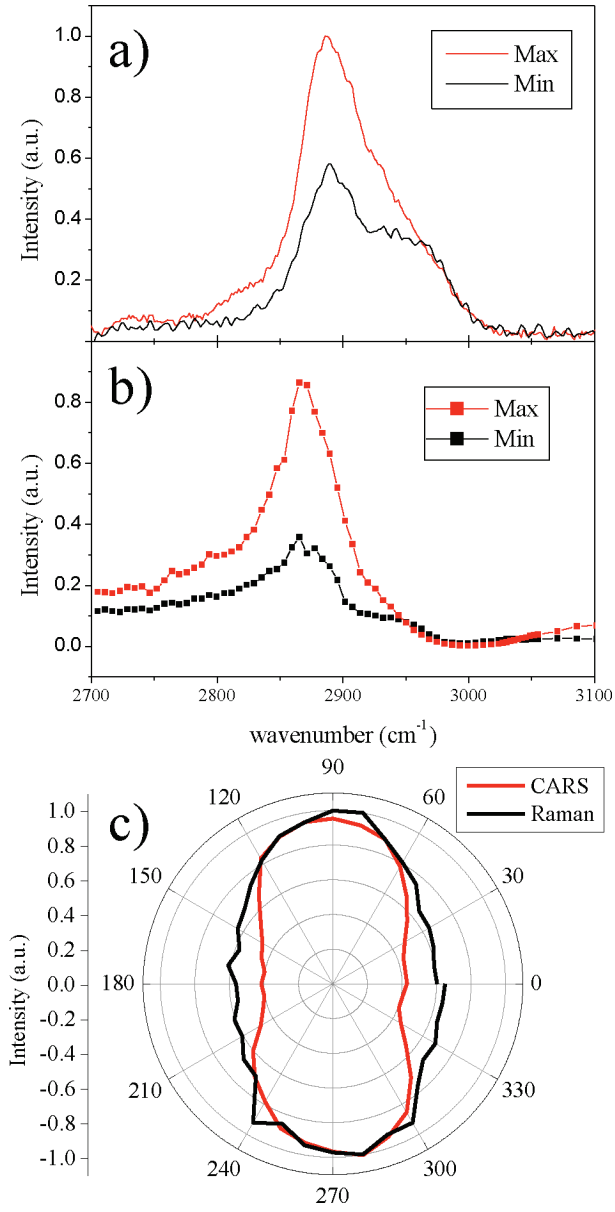

Figure 5. a) Raman spectrum of dry rayon. Red trace corresponds to fiber orientation with maximum Raman response, whereas black trace corresponds to the minimum response 90° rotated from the maximum. b) CARS spectrum of dry rayon. Red and black trace correspond to the same orientations as indicated in a). c) Polar plots of the CARS signal at 2880 cm^{-1} (red trace) and the 2890/2963 cm^{-1} ratio of the Raman intensity (black trace).

In addition to the main maximum, the CARS polarization plot shows a smaller local maximum oriented perpendicular to the main orientation of the mode. This feature is not reproduced in the Raman polarization plot. We attribute this second maximum to an enhanced anisotropic electronic contribution in the hydrated fiber. In CARS microscopy, this contribution is often referred to as the nonresonant background. In contrast to the nonresonant background observed in aqueous and liquid samples, the nonresonant electronic background in hydrated cellulose is not isotropic. In this scenario, the presence of water molecules in the cellulose microfibrils alters the electronic polarizability of the system in a well-defined direction. Although the magnitude of the electronic component varied somewhat with location in the fiber, we observed this phenomenon in all hydrated fibers tested ($n > 10$).

Figure 8 shows the Raman and CARS spectra of hydrated rayon. Similar to cotton, the spectra show limited changes upon hydration. As shown in the polarization plot in part c of Figure 8, the orientation of the methylene stretching mode is retained at 90° relative to the fiber axis. A strong electronic component is seen in rayon as well, directed along the main fiber axis, suggesting an ordered incorporation of interstitial water. The presence of this electronic component modifies the polarization-resolved CARS spectrum shown in part b of Figure 8, where a stronger mixing of the electronic background alters the spectrum in the direction orthogonal to the methylene stretching mode orientation.

The anisotropy and angular images shown in Figure 9 indicate that the anisotropy and orientation of the methylene mode is continuous throughout the fiber. The methylene mode is oriented persistently at 90° with respect to the fiber axis anywhere in the fiber. Note that this is true even if the rayon fiber is swollen by almost a factor of 2 upon hydration. The incorporation of water in the fiber has a limited effect on the average mode orientation in the cellulose units.

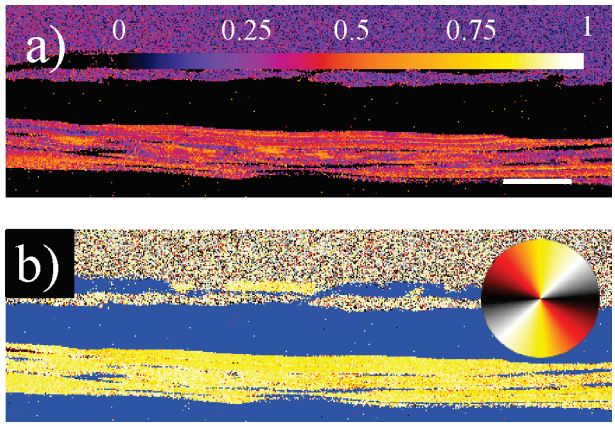

Figure 6. Anisotropy magnitude a) and director angle b) images of a dry rayon fiber determined at 2880 cm^{-1}. Scale bar is 35 μm.

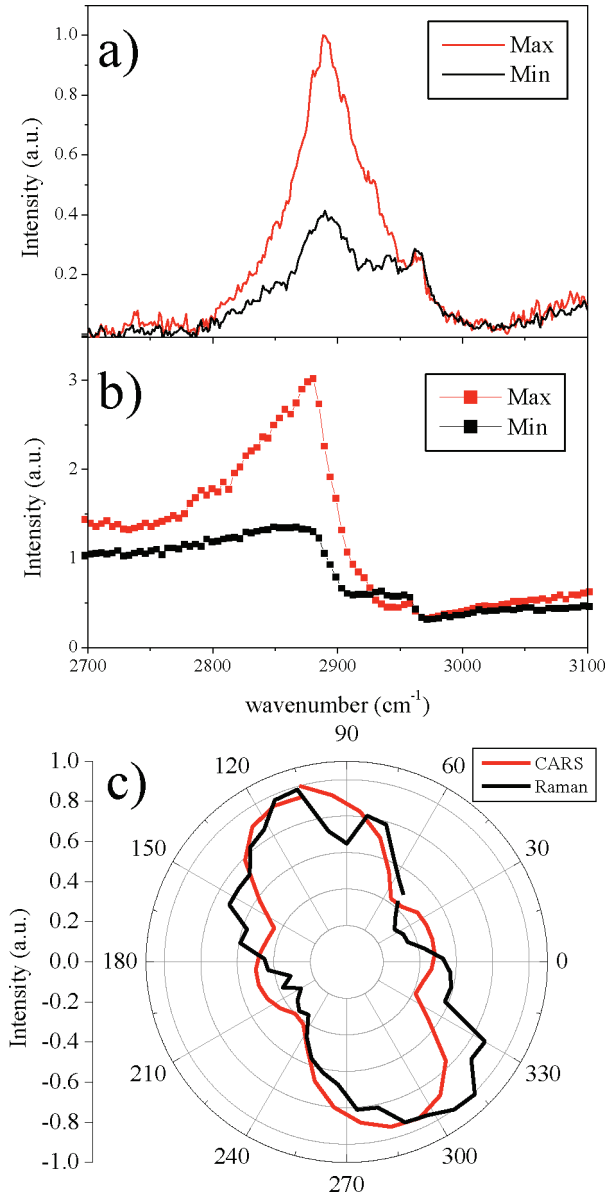

Figure 7. a) Raman spectrum of hydrated cotton. Red trace corresponds to fiber orientation with maximum Raman response, whereas black trace corresponds to the minimum response 90° rotated from the maximum. b) CARS spectrum of hydrated cotton. Red and black trace correspond to the same orientations as indicated in a). c) Polar plots of the CARS signal at 2880 cm^{-1} (red trace) and the 2890/2963 cm^{-1} ratio of the Raman intensity (black trace).

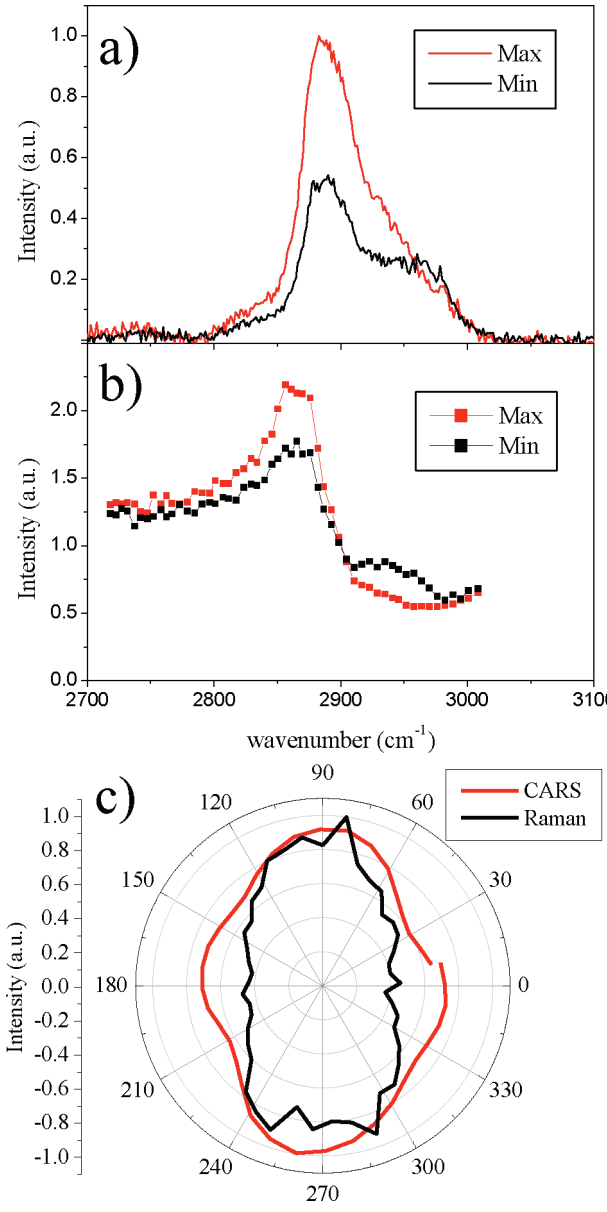

Figure 8. a) Raman spectrum of hydrated rayon. Red trace corresponds to fiber orientation with maximum Raman response, whereas black trace corresponds to the minimum response 90° rotated from the maximum. b) CARS spectrum of hydrated rayon. Red and black trace correspond to the same orientations as indicated in a). c) Polar plots of the CARS signal at 2880 cm^{-1} (red trace) and the 2890/2963 cm^{-1} ratio of the Raman intensity (black trace).

3.7. Electronic Polarizability in Hydrated Fibers. Figure 10 shows a comparison between the CARS polarization dependence and the SHG polarization dependence of a hydrated cotton fiber. The CARS polarization plot shows the characteristic two-lobed pattern. Here, the main maximum and the smaller lobed contribution are not completely orthogonally aligned. We attribute the smaller lobe pattern to the electronic contribution and the stronger maximum to the molecular mode, which may be orientated differently due to strain at this particular location in the fiber. Interestingly, the SHG polarization dependence aligns with the electronic contribution. This is a consistent trend, as the SHG maximum is found in the direction of the electronic nonresonant CARS component for all hydrated cotton fibers tested. We conclude that the enhanced third-order electronic polarizability in hydrated fibers has its major projection along

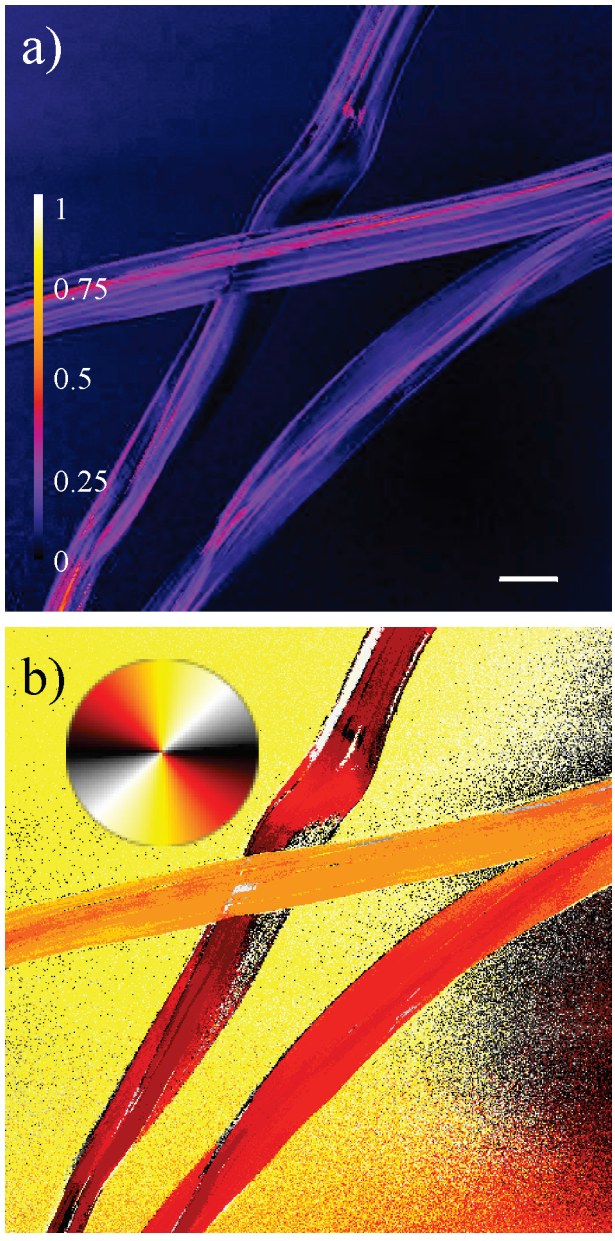

Figure 9. Anisotropy magnitude a) and director angle b) images for hydrated rayon. Scale bar is 35 μm.

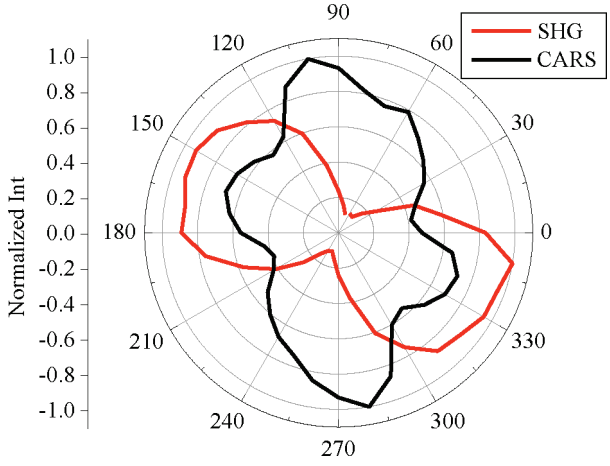

Figure 10. Comparison of the CARS angular dependence at 2880 cm^{-1} and the SHG angular dependence in hydrated cotton.

the polyglucan axis, in the same direction where the maximum of the second-order polarizability is found.

4. Conclusions

We have combined Raman and CARS with SHG measurements to elucidate the orientation of C−H stretching modes in dry and hydrated cellulose fibers. In cotton fibers, the average orientation of the methylene groups is persistent throughout fiber segments on the micrometer scale, indicating a high degree of order of the cellulose microfibrils on this length scale. At several locations, small micrometer-sized areas within the cotton fiber are seen in which the nonresonant electronic polarizability differs markedly with respect to the surrounding fiber material, possibly due to different packing of the cellulose microfibrils. In rayon fibers, the orientation of the methylene groups is highly conserved throughout the fiber, directed perpendicularly with respect to the fiber axis. The mode orientation is maintained upon hydration of the cotton and rayon fibers, indicating that the interstitial water has a limited effect on the overall alignment of the polyglucan chains. An anisotropic electronic contribution is seen in both cotton and rayon upon hydration of the fibers, suggesting an ordered incorporation of water molecules in the cellulose fibers. The second-order polarizability in cotton is found to be directed along the long axis of the polyglucan chains, and is dominated largely by the achiral component. The SHG measurements confirm furthermore the antiparallel arrangement of the polyglucan chains in rayon.

Acknowledgment. We thank Garth Simpson and Tyler Weeks for useful discussions. This work was supported by The Procter & Gamble Company. Any opinions, findings, and conclusions or recommendations expressed in this publication are those of the authors and do not necessarily reflect the official views of The Procter & Gamble Company. Equipment support was obtained from the National Science Foundation, grant DBI-0754624.

References and Notes

(1) Zugenmaier, P. *Crystalline Cellulose and Derivatives Characterization and Structures*; Springer: Berlin, 2008.

(2) Eichhorn, S. J.; Young, R. J.; Davies, G. R. Modeling Crystal and Molecular Deformation in Regenerated Cellulose Fibers. *Biomacromolecules* **2005**, *6*, 507–513.

(3) Northolt, M. G.; de Vries, H. Tensile Deformation of Regenerated and Native Cellulose Fibers. *Die Angewandte Makromolekulare Chemie* **1985**, *133*, 183–203.

(4) Chanzy, H.; Paillet, M. Hagège, Spinning of cellulose from N-methyl morpholine N-oxide in the presence of additives. *Polymer* **1990**, *31*, 400–405.

(5) Iyer, P. B.; Sreenivasan, S.; Chidambareswaran, P. K.; Batil, N. B.; Sundaram, V. Induced Crystallization of Cellulose in Never-Dried Cotton Fibers. *J. Appl. Polym. Sci.* **1991**, *42*, 1751–1757.

(6) Hu, X. P.; Hsieh, Y. L. Effects of Dehydration on the Crystalline Structure and Strength of Developing Cotton Fibers. *Text. Res. J.* **2001**, *71* (3), 231–239.

(7) Park, S.; Johnson, D. K.; Ishizawa, C. I.; Parilla, P. A.; Davis, M. F. Measuring the crystallinity index of cellulose by solid state ^{13}C nuclear magnetic resonance. *Cellulose* **2009**, *16*, 641–647.

(8) Gindl, W.; Reifferscheid, M.; Martinschitz, K. J.; Boesecke, P.; Keckes, J. Reorientation of Crystalline and Noncrystaline Regions in Regenerated Cellulose Fibers and Films Tested in Uniaxial Tension. *J. Appl. Polym. Sci.* **2007**, *46*, 297–304.

(9) Northolt, M. G.; Boerstoel, H.; Maatman, H.; Huisman, R.; Veurink, J.; Elzerman, H. The Structure and Properties of Cellulose Fibres Spun from an Anisotropic Phosphoric Acid Solution. *Polymer* **2001**, *42*, 8249–8264.

(10) Bakri, B.; Eichorn, S. J. Elastic Coils: Deformation Micromechanics of Coir and Celery Fibres. *Cellulose* **2010**, *17*, 1–11.

(11) Hinterstoisser, B.; Åkerholm, M.; Salmén, L. Effect of Fiber Orientation in Dynamic FTIR Study on Native Cellulose. *Carbohydr. Res.* **2001**, *334*, 27–37.

(12) Kong, K.; Eichorn, S. J. Crystalline and Amorphous Deformation of Process-Controlled Cellulose-II Fibers. *Polymer* **2005**, *46*, 6380–6390.

(13) Šturcová, A.; His, I.; Wess, T. J.; Cameron, G.; Jarvis, M. C. Polarized Vibrational Spectroscopy of Fiber Polymers: Hydrogen Bonding in Cellulose II. *Biomacromolecules* **2003**, *4*, 1489–1595.

(14) Gindl, W.; Martinschitz, K. J.; Boesecke, P.; Keckes, J. Orientation of Cellulose Crystallites in Regenerated Cellulose Fibers under Tensile and Bending Loads. *Cellulose* **2006**, *13*, 621–627.

(15) Kong, K.; Davies, R. J.; McDonald, M. A.; Young, R. J.; Wilding, M. A.; Ibbett, R. N.; Eichhorn, S. J. Influence of Domain Orientation on the Mechanical Properties of Regenerated Cellulose Fibers. *Biomacromolecules* **2007**, *8*, 624–630.

(16) Eichorn, S. J.; Young, R. J.; Davies, R. J.; Riekel, C. Characterisation of the Microstructure and Deformation of High Modulus Cellulose Fibers. *Polymer* **2003**, *44*, 5901–5908.

(17) Tsuboi, M. Infrared Spectrum and Crystal Structure of Cellulose. *J. Polym. Sci.* **1957**, *25*, 159–171.

(18) Atalla, R. H.; Whitmore, R. E.; Heimbach, C. J. Raman Spectral Evidence for Molecular Orientation in Native Cellulosic Fibers. *Macromolecules* **1980**, *13*, 1717–1719.

(19) Gierlinger, N.; Luss, S.; König, C.; Konnerth, J.; Eder, M.; Fratzl, P. Cellulose Microfibril Orientation of *Picea abies* and its Variability at the Micron-Level Determined by Raman Imaging. *J. Exp. Bot.* **2009**, *61* (2), 587–595.

(20) Fischer, S.; Schenzel, K.; Fischer, K.; Diepenbrock, W. Applications of FT Raman Spectroscopy and Micro Spectroscopy Characterizing Cellulose and Cellulosic Biomaterials. *Macromol. Symp.* **2005**, *223*, 41–56.

(21) Wiley, J. H.; Atalla, R. H. Band Assignments in the Raman Spectra of Celluloses. *Carbohydr. Res.* **1987**, *160*, 113–129.

(22) Cheng, J. X.; Xie, X. S. Coherent Anti-Stokes Raman Scattering Microscopy: Instrumentation, Theory and Applications. *J. Phys. Chem. B* **2004**, *108*, 827–840.

(23) Evans, C. L.; Xie, X. S. Coherent Anti-Stokes Raman Scattering Microscopy: Chemical Imaging for Biology and Medicine. *Annu. Rev. Anal. Chem.* **2008**, *1*, 883–909.

(24) Potma, E. O.; Xie, X. S. Theory of Spontaneous and Coherent Raman scattering. In *Handbook of Biological Nonlinear Optical Microscopy*; Masters, B. R., So, P. T. C., Eds.; Oxford University Press: New York, 2008; pp 164−185.

(25) Potma, E. O.; Xie, X. S. Detection of Single Lipid Bilayers with Coherent Anti-Stokes Raman Scattering (CARS) Microscopy. *J. Raman Spectrosc.* **2003**, *34*, 642–650.

(26) Wurpel, G. W. H.; Rinia, H. A.; Muller, M. Imaging Orientational Order and Lipid Density in Multilamellar Vesicles with Multiplex CARS Microscopy. *J. Microsc.* **2005**, *218*, 37–45.

(27) Saar, B. G.; Park, H.; Xie, X. S.; Lavrentovich, O. D. Three-Dimensional Imaging of Chemical Bond Orientation in Liquid Crystals by Coherent Anti-Stokes Raman Scattering Microscopy. *Opt. Express* **2007**, *15* (21), 13585–13596.

(28) Kachynski, A. V.; Kuzmin, A. N.; Prasad, P. N.; Smalyukh, I. I. Coherent anti-Stokes Raman Scattering Polarized Microscopy of Three-Dimensional Director Structures in Liquid Crystals. *Appl. Phys. Lett.* **2007**, *91*, 151905.

(29) Brown, R. M. J.; Millard, A. C.; Campagnola, P. J. Macromolecular Structure of Cellulose Studied by Second-Harmonic Generation Imaging Microscopy. *Opt. Lett.* **2003**, *28* (22), 2207–2209.

(30) Marubashi, Y.; Higashi, T.; Hirakawa, S.; Tani, S.; Erata, T.; Takai, M.; Kawamata, J. Second Harmonic Generation Measurements for Biomacromolecules: Celluloses. *Opt. Rev.* **2004**, *11* (6), 385–387.

(31) Munhoz, F.; Brustlein, S.; Gachet, D.; Billard, F.; Brasselet, S.; Rigneault, H. Raman Depolarization Ratio of Liquids Probes by Linear Polarization Coherent Anti-Stokes Raman Spectroscopy. *J. Raman Spectrosc.* **2009**, *40* (7), 775–780.

(32) Wiley, J. H.; Atalla, R. H. Band Assignments in the Raman Spectra of Celluloses. *Carbohydr. Res.* **1987**, *160*, 113–129.

(33) Pizzini, S.; Bajo, G.; Abbate, S.; Conti, G.; Atalla, R. H. Assessment of the Values of the C-H Stretching Force Constants in Sugar Molecules. *Carbohydr. Res.* **1988**, *184*, 1–11.

(34) Langan, P.; Nishiyama, Y.; Chanzy, H. X-ray Structure of Mercenized Cellulose II at 1 Å Resolution. *Biomacromolecules* **2001**, *2*, 410–416.

(35) Rocha-Mendoza, I.; Yankelevich, D. R.; Wang, M.; Reiser, K. M.; Frank, C. W.; Knoesen, A. Sum Frequency Vibrational Spectroscopy: The Molecular Origins of the Optical Second-Order Nonlinearity of Collagen. *Biophys. J.* **2007**, *93*, 4433–4444.

(36) Gualtieri, E. J.; Haupert, L. M.; Simpson, G. J. Interpreting Nonlinear Optics of Biopolymer Assemblies: Finding a Hook. *Chem. Phys. Lett.* **2008**, *465*, 167–174.

JP103216J